THEORETICAL AND APPLIED MECHANICS
Volume 45 (2018) Issue 1, 83–94 DOI: https://doi.org/10.2298/TAM171130006B

ENERGY SEPARATION IN TRANSIENT AND STEADY-STATE FLOW ACROSS THE CYLINDER

Jela M. Burazer

Abstract. Energy separation is a spontaneous energy redistribution within a fluid flow. As a consequence, there are places with higher and lower values of total temperature in the fluid flow. It is characteristic for many flow geometries. This paper deals with the energy separation in a cylinder wake. Two flow conditions are being considered–transient and steady-state flow in the wake. Two different solvers from the open source package OpenFOAM are used in order to capture the phenomenon of energy separation. One of these solvers is modified for the purpose of calculation in a particular case of the vortex street flow. The energy equation based on the internal energy present in this solver is replaced by the energy equation written in the form of a total enthalpy. The other solver has been previously tested in the vortex tube flow, and can also capture the energy separation in the steady-state wake flow of the cylinder. In both cylinder wake flow conditions, a two-dimensional computational domain is used. Standard $k-\varepsilon$ model is used for computations. It is proved that OpenFOAM is capable of capturing the energy separation phenomenon in a proper way in both of the wake flow cases. Good agreement between the experimental results and the ones from computations is obtained in the case of steady-state flow in the wake. Previous research findings are also confirmed in the case of vortex street flow.

1. Introduction

Energy separation i.e., total temperature separation, is a spontaneous process of total energy redistribution within a fluid flow, in the way that in the part of the flow field total temperature is higher, while in the other part it is lower than in the start of the flow. Total temperature separation was first noticed in the 1930s in a vortex tube, and later, it was noticed in wakes of bluff bodies, in shear layers, in jets, wakes of turbine blades... In spite of a great deal of experimental, numerical and theoretical research reported over the years, there is still no clear conclusion regarding the cause and mechanism of the energy separation phenomenon.

2010 *Mathematics Subject Classification:* 76F10.
Key words and phrases: energy separation, cylinder, OpenFOAM, turbulence, compressible flow.

The first papers regarding the energy separation in a cylinder wake are [1] and [2]. There it was noticed that if there is a bluff body inside a fluid flow, the temperature of the rearmost point of the body has lower total temperature than it was upstream. Ryan [3] afterwards noticed that, apart from the lower total temperature on the surface of the bluff body, the temperature drop extends downstream the wake as well. Thomann [4] showed that the attachment of the splitter plate behind a wedge leads to an increase in the total temperature around its rearmost point, while suppressing the vortex street. Goldstein and He [5] obtained similar results. They also postulated that if the frequency which causes the velocity of the fluid flowing past the cylinder is very close to the frequency of the tunnel, an increase in vortex shedding occurs, and lower temperatures are obtained in the cylinder's wake. Kurosaka et al. [6] increased the vortex shedding through acoustic synchronization – resonance between the vortex shedding and transversely standing acoustic waves in the wind tunnel. They postulated that vortex shedding is indeed the cause of the temperature separation phenomenon. Ng and Chakroun [7] measured total temperature field and pressure in the wake behind the cylinder. The reported temperature drop in the cylinder wake was 15 K. It is established that the minima and maxima of the total temperature and total pressure coincide in the flow field. Goldstein and Kulkarni [8] and Kulkarni and Goldstein [9] reported the results of the averaged total temperature and velocity fields. They found that the vortices that detach from the back of the cylinder are slowly decreasing in their size. Time-resolved measurements of total temperature and pressure in the cylinder wake were performed in [10]. They confirmed the presence of energy separation. Numerical computations were performed as well, which showed lower total temperature in the wake's centerline and higher values of this quantity in the neighboring regions.

This paper deals with the energy separation in a cylinder wake. Two flow conditions are being considered–transient and steady-state flow in the wake. Two different solvers from the open source package OpenFOAM are used in order to capture the phenomenon of energy separation. One of these solvers is modified for the purpose of calculation in a particular case of the vortex street flow. In this paper, experimental results from [8] are used in order to validate the ability of a newly developed solver to capture energy separation in the cylinder wake, in the case with no vortices detaching from the cylinder. The same geometry and boundary conditions are used for energy separation research in the vortex street flow.

2. Mathematical models

2.1. Governing equations. The fluid flow considered in this paper is compressible and turbulent. Since there are gradients of temperature in both axial and radial direction, energy equation is also solved, together with the continuity and momentum equations. Governing equations are written in terms of Favre's mass weighted averages, [12]. Here, any of the dependent variables f is decomposed into mean $\tilde{f}$ and fluctuating part f'', i.e., $f = \tilde{f} + f''$. In Favre's averaging the following equality stands: $\widetilde{\varrho f''} = 0$. Hence, the mean value of variable f in terms of Favre

averaging is $\langle\varrho\rangle\tilde{f} = \langle\varrho f\rangle$. Following are the Favre averaged Navier–Stokes (FANS) equations written in invariant form:

$$\frac{\partial\langle\varrho\rangle}{\partial t} + \nabla\cdot(\langle\varrho\rangle\tilde{\underline{u}}) = 0,$$

$$\frac{\partial(\langle\varrho\rangle\tilde{\underline{u}})}{\partial t} + \nabla\cdot(\langle\varrho\rangle\tilde{\underline{u}}\otimes\tilde{\underline{u}}) = -\nabla\langle p\rangle + \nabla\cdot(\langle\underline{\underline{T}}\rangle - \langle\varrho\underline{u}''\otimes\underline{u}''\rangle),$$

as well as the Favre averaged energy equation:

$$\begin{aligned}\partial_t(\langle\varrho\rangle\tilde{H}) + \nabla\cdot(\langle\varrho\rangle\langle H\rangle\tilde{\underline{u}}) = \frac{\partial\bar{p}}{\partial t} + \nabla\cdot[-\langle\varrho\underline{u}''h''\rangle + \langle\underline{\underline{T}}\cdot\underline{u}''\rangle - \langle\varrho\underline{u}''\tfrac{1}{2}\underline{u}''\cdot\underline{u}''\rangle]\\ + \nabla\cdot[\tilde{\underline{u}}\cdot(\langle\underline{\underline{T}}\rangle - \langle\varrho\underline{u}''\otimes\underline{u}''\rangle)] - \nabla\cdot\tilde{\underline{q}},\end{aligned}$$

where ∂_t is the time derivative of the $\langle\varrho\rangle\tilde{H}$. This system of equations is not closed. In order to accomplish that, constitutive relations that are also Favre averaged are used:

$$\begin{aligned}\langle\underline{\underline{T}}\rangle &= \mu\big\{\big[\nabla\tilde{\underline{u}} + (\nabla\tilde{\underline{u}})^T\big] - \tfrac{2}{3}(\nabla\cdot\tilde{\underline{u}}'')\underline{\underline{I}}\big\} + \mu\big\{\big[\nabla\langle\underline{u}''\rangle + (\nabla\langle\underline{u}''\rangle)^T\big] - \tfrac{2}{3}(\nabla\cdot\langle\underline{u}''\rangle)\underline{\underline{I}}\big\}\\ &= \underline{\underline{\tau}} + \langle\underline{\underline{\tau}}''\rangle \cong \underline{\underline{\tau}},\end{aligned}$$

$$\langle p\rangle = \langle\varrho\rangle R\tilde{T}, \quad \tilde{H} = \tilde{h} + \frac{\tilde{\underline{u}}\cdot\tilde{\underline{u}}}{2} + \frac{1}{2}\langle\underline{u}''\cdot\underline{u}''\rangle, \quad \tilde{h} = c_p\tilde{T}, \quad \tilde{\underline{q}} = -\lambda\nabla\tilde{T}.$$

The dyad $-\langle\varrho\underline{u}''\otimes\underline{u}''\rangle \equiv \underline{\underline{R}}$ which appears in averaged equations is the Favre-averaged Reynolds stress tensor. Together with the second term on the right hand side of the energy equation, it is a new unknown quantity in Favre averaged Navier–Stokes equations. Reynolds stresses are modelled by turbulent models. Standard $k-\varepsilon$ model is used in this paper. The unknown in the energy equation consists of the turbulent transport of heat $\langle\varrho\underline{u}''h''\rangle$, molecular diffusion $\langle\underline{\underline{T}}\cdot\underline{u}''\rangle$ and turbulent transport $-\langle\varrho\underline{u}''\frac{1}{2}\underline{u}''\cdot\underline{u}''\rangle$. Following the analogy between momentum and heat transfer, the turbulent heat-flux vector is proportional to the mean temperature gradient, as follows:

$$\underline{q}_t = \langle\varrho\underline{u}''h''\rangle = -\frac{\mu_{\mathrm{T}}}{\mathrm{Pr}_{\mathrm{T}}}\nabla h'',$$

where Pr_{T} is the turbulent Prandtl number.

On the other hand, the most commonly used approximation for the last two unknown terms in the energy equation is:

$$\langle\underline{\underline{T}}\cdot\underline{u}''\rangle - \langle\varrho\underline{u}''\tfrac{1}{2}\underline{u}''\cdot\underline{u}''\rangle = \Big(\mu + \frac{\mu_{\mathrm{T}}}{\sigma_k}\Big)\nabla k.$$

Here, σ_k is a constant, whose value depends on the turbulence model used for turbulent viscosity calculation.

It is important to note that the concept of Favre averaging is purely mathematical. It was introduced so that the governing equations of turbulent compressible flow (FANS) are written in a similar way to those of the turbulent incompressible flow (RANS). The aim is that the influence of density changes on the flow variables is present in the equations that describe the flow. However, by means of Favre averaging procedure, fluctuations due to density changes are omitted from the governing equations, [13].

2.2. Modeling of compressible turbulent flow. Out of all turbulence models present in turbulence research, standard $k-\varepsilon$ model is chosen for this study. This model relies on the Boussinesq hypothesis, which for compressible flow has the following form:

$$-\varrho\langle \underline{u}\otimes\underline{u}\rangle = \mu_{\mathrm{T}}\big(2\underline{\underline{S}} - \tfrac{2}{3}(\nabla\cdot\underline{u})\underline{\underline{I}}\big) - \tfrac{2}{3}\varrho k\underline{\underline{I}}.$$

The dynamic eddy viscosity is calculated via

$$\mu_{\mathrm{T}} = C_\mu \varrho \frac{k^2}{\varepsilon+\varepsilon_{\mathrm{small}}},$$

where $\varepsilon_{\mathrm{small}} = 10^{-15}$, is introduced for avoiding division with zero, and constant $C_\mu = 0.09$. Transport equations for kinetic energy of turbulence and energy dissipation in standard $k-\varepsilon$ model are as follows:

$$\frac{\partial}{\partial t}(\varrho k) + \nabla\cdot(\varrho k\underline{u}) = \mu_{\mathrm{T}}\nabla\underline{u} : \big(2\underline{\underline{S}} - \tfrac{2}{3}(\nabla\cdot\underline{u})\underline{\underline{I}}\big) - \varrho\varepsilon - \tfrac{2}{3}\varrho k\nabla\cdot\underline{u} + \nabla\cdot\Big(\Big(\mu+\frac{\mu_{\mathrm{T}}}{\sigma_k}\Big)\nabla k\Big),$$

and

$$\frac{\partial}{\partial t}(\varrho\varepsilon) + \nabla\cdot(\varrho\varepsilon\underline{u}) = \nabla\cdot\Big(\Big(\mu+\frac{\mu_{\mathrm{T}}}{\sigma_\varepsilon}\Big)\nabla\varepsilon\Big) + C_1\frac{\varepsilon}{k}\big(\mu_{\mathrm{T}}\nabla\underline{u} : \big(2\underline{\underline{S}} - \tfrac{2}{3}(\nabla\cdot\underline{u})\underline{\underline{I}}\big)\big) - C_2\frac{\varrho\varepsilon^2}{k} - \big(\tfrac{2}{3}C_1 + C_3\big)\varrho\varepsilon\nabla\cdot\underline{u}.$$

The constants in this model have the following values: $C_1 = 1.44$, $C_2 = 1.92$, $C_3 = -0.33$, $\sigma_\varepsilon = 1.3$, $\sigma_k = 1$. All constants are taken from [13].

3. Numerical procedure

3.1. Computational domain and mesh. The case of the flow across the cylinder from [8] is the test case for rhoCentralTurbFoam solver. The ability of this solver to predict the energy separation in the particular case of the wake flow is examined. Namely, this solver, as will be explained later, predicts the total temperature separation in the steady-state cylinder wake flow. The problem is considered to be two-dimensional. A non-uniform, blockstructured mesh is created using a mesh generator blockMesh, inbuilt within OpenFOAM. A sketch of the computational domain is presented in Figure 1. The cylinder is located in the channel of the rectangular cross section with dimensions $L_k \times H$. The dimensions presented in this figure are as follows: $L = 1286.2\,\mathrm{mm}$, $H = 203\,\mathrm{mm}$, $L_k = 101.5\,\mathrm{mm}$, $D = 19.5\,\mathrm{mm}$, $\ell = 60\,\mathrm{mm}$.

The mesh is body-fitted around the cylinder and proportional grid grading is employed in the areas of the flow where high gradients of physical quantities are expected. Since standard $k-\varepsilon$ model for turbulence closure is used, care is taken that the y+value is approximately 30 near all the walls. This is confirmed after calculations are completed.

There are no appropriate experimental results for the other solver, sonicTEFoam. Namely, this newly developed solver predicts the energy separation in the

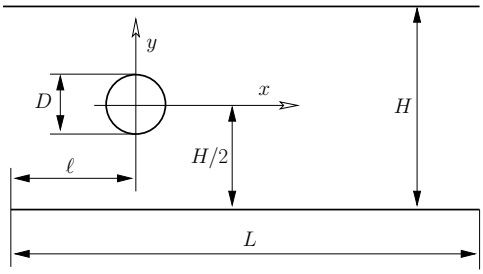

FIGURE 1. Sketch of the computational domain.

vortex street flow. However, there are certain findings from previous research, regarding the energy separation in vortices, as well as their influence on the energy separation intensity, that can be confirmed here. The same geometry and the same boundary conditions are used for both solvers.

3.2. Boundary conditions. The boundary conditions are set as follows: fixed value of the velocity in the axial direction is set on the inlet, while for the pressure Neumann boundary condition is set. At the outlet, a Neumann boundary condition is set for the velocity, and for the pressure a fixed value is adopted. The static temperature value is also known at the inlet. Hence the fixed value boundary condition is set here, while at the outlet the Neumann condition is set for this quantity. A no-slip boundary condition is set for the velocity, while for the other quantities the Neumann is used on the walls. Since two-equation model is used in this research, wall functions are used on this boundary of the computational domain for turbulence quantities. The cylinder is adiabatic and motionless. For the sonicTEFoam solver, a boundary condition for total enthalpy has to be set also. The fixed value of this quantity is set on the inlet, while on the outlet and on the walls the Neumann is set. The value of Mach number at the inlet is M = 0.23. Values for all fixed value boundary conditions are taken from [8].

3.3. Numerical solvers. The foam-ext-3.1 version of the open-source software OpenFOAM is used in this research. Two different solvers, both compressible, transient and density based, are used: rhoCentralTurbFoam and sonicTEFoam. Each of the solvers predicts the energy separation in certain flow conditions in the cylinder wake. Namely, rhoCentralTurbFoam in steady-state flow (Figure 2a), and when the vortex street is present–sonicTEFoam (Figure 2b). Previous versions of these two solvers, in original form named rhoCentralFoam and sonicFoam, could not resolve turbulent flows, and could not capture energy separation phenomenon present in the flow, respectively. Details will be presented further on.

Solver rhoCentralTurbFoam is intended for high speed viscous flows calculations. Burazer et al. [11] added the ability to resolve turbulent flows, compiled it as a solver with aforementioned name and carried on using it for turbulent high speed viscous flow computations. This solver is based on semidiscrete, non-staggered central schemes of Kurganov and Tadmor [16] and Kurganov et al. [17]. Details about the implementation of these schemes in this solver can be found in [18].

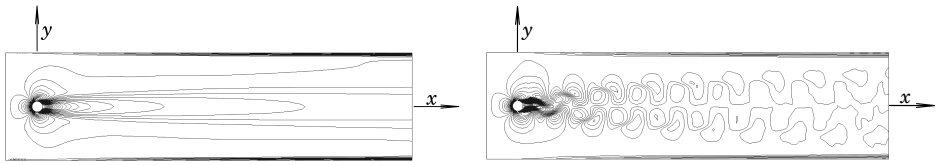

(A) (B)

FIGURE 2. The flow conditions in which the total temperature separation is predicted by the use of (A) rhoCentralTurbFoam and (B) sonicTEFoam .

In short, rhoCentralTurbFoam solver solves each of the governing equations separately. In the first step, density is calculated from the continuity equation, while using the values of the velocity from the previous step. Next, the momentum equation is being solved. This is done in two steps. First, the inviscid momentum density $\varrho\underline{\tilde{u}}$ is calculated. Then, since density and momentum density are known, an intermediate estimation of the velocity value can be determined. Finally, a diffusion correction equation for velocity field $\underline{\tilde{u}}$ is solved, velocity value is calculated and the $\varrho\underline{\tilde{u}}$ is updated. The same procedure is applied for the energy equation. First energy density $\varrho\underline{\tilde{E}}$ is calculated, and afterwards the total energy taking into account the diffusive heat flux also. Knowing the values of velocity and total energy, the value of internal energy e can be determined. Finalising the loop, values of e and $\varrho\underline{\tilde{E}}$ are updated, while pressure field is calculated from the equation of state.

Solver sonicTEFoam is obtained by modifying the sonicFoam solver [19], already present in the foam-ext-3.1 version of the OpenFOAM software. The energy equation based on the internal energy is replaced by an energy equation written in the form of the total enthalpy. Additionaly local time stepping is implemented in the sonicTEFoam solver which makes the computations more stable. The sonicTEFoam solver relies on the PISO alghorithm in its calculations. More details about solution alghorithms can be found in Refs. [14] and [15]. The calculation starts in an outer loop with the values of the assumed density field. Using those, the momentum and energy equations are solved for velocity and enthalpy fields. The values of the velocity at this stage of the calculation do not satisfy the continuity equation. In order to accomplish that, a pressure-correction procedure of the PISO algorithm is used. After additional loops in the aforementioned algorithm have been performed, the pressure value is corrected, the continuity equation is satisfied, and at the end, the density is updated using the equation of state.

Since the local time stepping is implemented within both of the solvers, the time step size is controlled by the maximum value of the Co number. In all of the computations, this value is 0.3. In the beginning of the calculations, the discretizations of the convective schemes are kept at the first order of accuracy. Afterwards, they were changed, and the calculations are finished with the accuracy of the second order. The tolerances for matrix solvers are as follows: in rhoCentralTurbFoam the tolerance for the velocity field is 10^{-9}, for turbulence quantities and internal energy the tolerance is the same: 10^{-10}; in sonicTEFoam the tolerance for all fields are

10^{-8}. In both solvers, the relative tolerance is set to zero. In that way all results are forced to converge to their imposed tolerances in each time step. The air is treated as a calorically perfect gas with constant values of the dynamic viscosity and the laminar Prandtl number: $\mu = 1.8 \times 10^{-5}\,\mathrm{N/(m^2 s)}$, $\mathrm{Pr} = 0.7$.

4. Results and discussion

4.1. Steady-state flow. Energy separation in steady-state flow across the cylinder is captured with rhoCentralTurbFoam solver. The comparison of the experimental [8] and numerically obtained values of the velocity in the channel is shown in Figure 3.

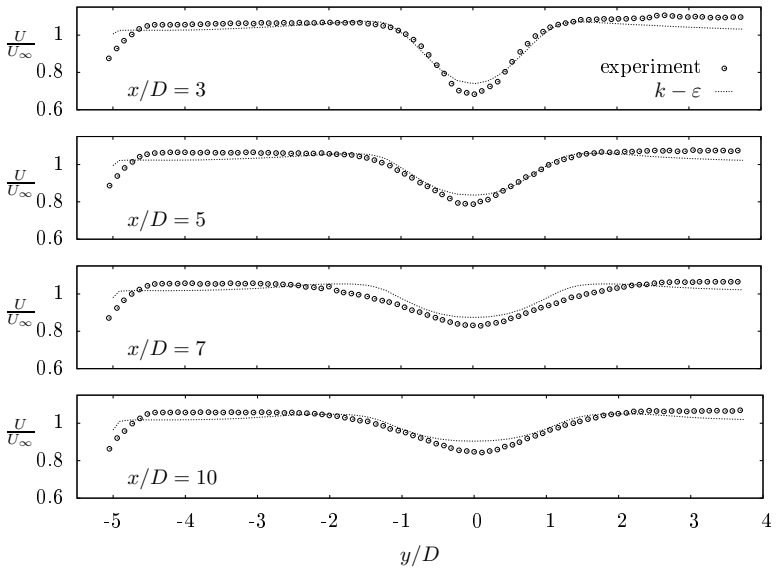

FIGURE 3. The distribution of the dimensionless axial velocity compared between the experimental [8] and computationally obtained values, rhoCentralTurbFoam solver, $k-\varepsilon$ model.

There is good agreement between the experimental and numerically obtained results. As expected in this kind of flow, the velocity profile is deformed in the cylinder wake. It is evident that the deformation of the velocity profile is getting smaller with the increase of the distance from the cylinder. The distribution of total temperature in the four cross sections downstream the cylinder is presented in Figure 4. The best agreement between the experiment and the results obtained from the rhoCentralTurbFoam solver is in the first cross section considered, i.e., in cross section $x/D = 3$. Afterwards the coincidence is diminishing. One of the reasons for this discrepancy between the results can be found in the difference in predicting the turbulence intensity, [19]. Turbulence intensity is underpredicted in all of the cross sections, except in the cross section $x/D = 3$. The increase in

the distance between the cylinder and the cross section in stake is followed by an increase in the difference in respect to the experimental values regarding this quantity. However, the agreement between the experimental and numerical results is very good. The greatest difference between the experimental and numerical results regarding the total temperature in the axis of the cylinder is of the order of 1K.

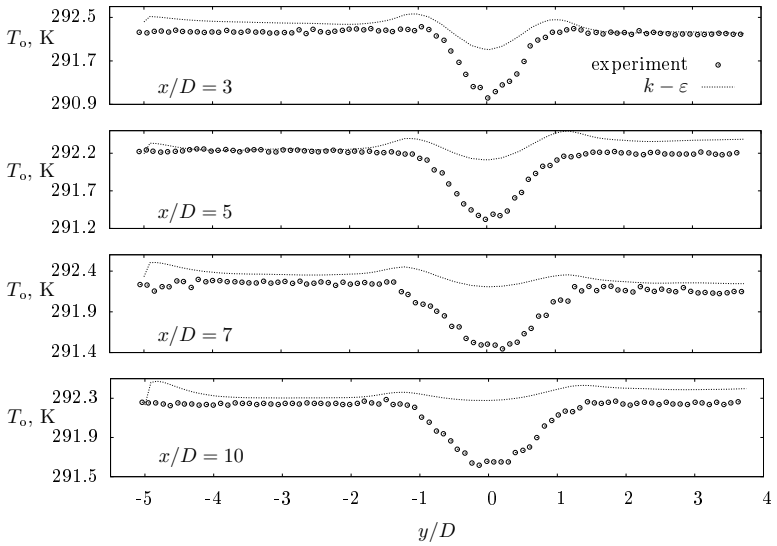

FIGURE 4. The comparison between the experimental [8] and numerically obtained values of total temperature, rhoCentralTurbFoam solver, $k - \varepsilon$ model.

4.2. Transient flow. Energy separation in the wake of the cylinder when vortex street is present is predicted by the sonicTEFoam solver. The total temperature distribution in the cylinder wake is presented in Figures 5 and 6. It is evident that there are hot and cold spots in the flow field in a chess distribution. This distribution is following the distribution of the vortices that are formed in the flow field.

This is even more evident from Figure 6. Here the total temperature distribution in the cylinder wake is presented together with the contours of the axial velocity. It is clear that the minimum of the axial velocity and the minimum of the total temperature are present at the same locations in the fluid flow domain. Hence, each vortex is thermally separated, as reported in [6]. However, the static temperature doesn't follow this pattern. It has a minimum in the central line of the channel, after which its value raises towards the walls of the channel. The distribution of static temperature is shown in Figure 5.

4.3. Influence of vortex shedding on energy separation. Since the same geometry and boundary conditions are used for both transient and steady-state flow in the cylinder wake, numerical analysis of the vortex shedding influence on the energy separation intensity can be performed. This analysis is performed here

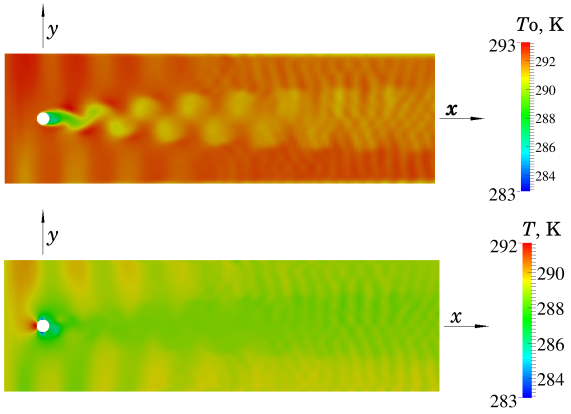

FIGURE 5. Total (T_o) and static (T) temperature distributions in the cylinder wake, sonicTEFoam, $k-\varepsilon$

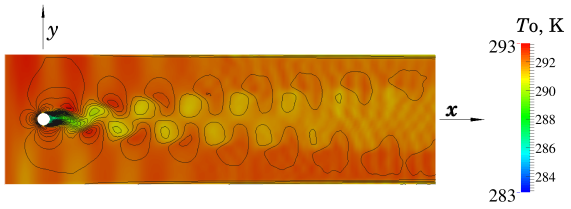

FIGURE 6. Axial velocity contours with total temperature field in the vortex street flow, sonicTEFoam solver, $k-\varepsilon$ model.

with the use of Figure 7, where distributions of the energy separation factor S in the channel centerline is presented. Energy separation factor is a dimensionless value of total temperature defined as:

$$S = \frac{T_o - T_{o,0}}{U^2/(2c_p)},$$

where the quantity in the denominator stands for the dynamic temperature, U is the air velocity, c_p is the specific heat, T_o is the total temperature, and $T_{o,0}$ is the total temperature at the inlet.

The values that correspond to the steady-state flow in the cylinder wake are those from the experiment [8] and numerical results of the rhoCentralTurbFoam solver. The sonicTEFoam solver results are the values of the energy separation factor in the vortex shedding wake flow.

Figure 7 confirms the slight difference in the energy separation prediction by the rhoCentralTurbFoam solver, already presented in Figure 4. What is important is the fact that the sonicTEFoam is predicting lower values of the energy separation factor. This is the consequence of vortex shedding, as reported by the experimental research in Refs. [4] and [5]. The influence of the proximity of the cylinder, i.e., of

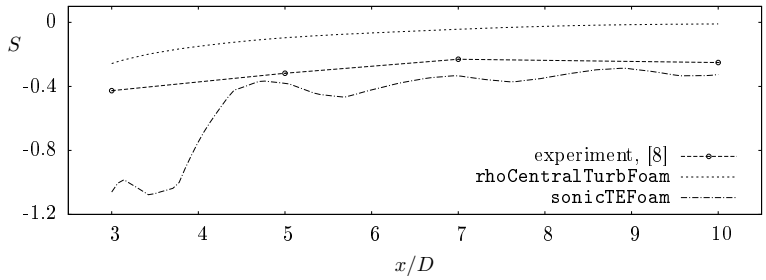

FIGURE 7. Distributions of energy separation factor S in the channel centerline, steady-state and transient flow: experiment [8], rhoCentralTurbFoam and sonicTEFoam solvers, $k-\varepsilon$ model.

the size of the vortices detaching from it, is evident. The vortices are slowly decreasing in their size downstream, as reported in Refs. [8] and [9]. Greater vortices are responsible for greater temperature drop, i.e., lower value of the energy separation factor, (see Figure 7). The total temperature is increasing in the wake centerline downstream the cylinder, as the size of the vortices is decreasing. Therefore there is an asymptotic, slow, approach of the energy separation factor curve predicted by the sonicTEFoam solver to the constant value, as presented in the Figure 7. Still, this constant value of the energy separation factor far from the cylinder is smaller than the one obtained in the experiment without the vortex shedding in the cylinder wake [8].

5. Conclusions

The results of the computational research of the total temperature separation in the cylinder wake are presented in this paper. Compressible solver is modified so that the energy separation in the vortex street flow could be captured. The other solver used in the research already performed well in the vortex tube energy separation computations. Its energy separation prediction ability is also confirmed in the steady-state cylinder wake flow. This is important for the research of the energy separation mechanism presented in these flow fields.

Two flow conditions in the cylinder wake are considered in this paper. For each of it, different solver predicts the total temperature separation. The energy separation phenomenon is captured in both cases. In the case of the steady-state flow, experimental and numerically obtained results of the velocity are in fairly good agreement. The agreement in the total temperature experimental and numerical values is also good. In the case of the vortex street in the cylinder wake there are no experimental results to compare with. However, from previous research there are certain findings that are confirmed in this paper. The minimum values of the velocity and those of the total temperature occur at the same places in the fluid flow. It is confirmed that the prevention of the vortex shedding is followed by the total temperature rise in the cylinder wake. The vortices size proved to be important in the energy separation mechanism. The presence of greater vortices in the fluid flow is followed by lower value of the energy separation factor.

The implementation of the total enthalpy energy equation in the sonicFoam solver proved to be efficient, since the energy separation is successfully predicted in the vortex street flow. Local time stepping is also successfully implemented in the same solver, which facilitated the control over the time step size during the computations, and improved their stability.

Acknowledgments. This work was funded by the grant from the Ministry of Education, Science and Technological Development, Republic of Serbia through project TR35046, what is gratefully acknowledged.

References

1. E. R. G. Eckert, A. Weise, *Messungen der Termperaturerteilung auf der Oberfläche Schnell Angeströmter Unbeheizter Körper*, Forsch. Gebiete Ingenieurwes. **13**(6) (1942), 246–254.
2. E. R. G. Eckert, *Experiments on Energy Separation in Fluid Streams*, Mechanical Engineering **106**(10) (1984), 58–64.
3. L. F. Ryan, *Experiments in Aerodinamic Cooling*, PhD Thesis, ETH Zürich, 1951.
4. H. Thomann, *Measurements of the recovery temperature in the wake of a cylinder and of a wedge and Mach number between 0.5 and 3*, F.F.A. Rept. 84, 1959, Stockholm, Sweden.
5. R. J. Goldstein, B. He, *Energy separation and acoustic interaction in flow across a circular cylinder*, Journal of Heat Transfer, Transactions of ASME **123** (2001), 682–687.
6. M. Kurosaka, J. B. Gertz, J. E. Graham, J. R. Goodman, P. Sundaram, W. C. Riner, H. Kuroda, W. L. Hankey, *Energy separation in a vortex street*, J. Fluid Mech. **178** (1987), 1–29.
7. W. F. Ng, W. M. Chakroun, *Time-resolved measurements of total temperature and pressure in vortex street behind a cylinder*, Phys. Fluids, A **2**(6) (1990), 971–978.
8. R. J. Goldstein, K. S. Kulkarni, *Energy separation in the wake of a cylinder*, Journal of Heat Transfer, Transactions of ASME **130** (2008), 061706-1–061706-9.
9. K. S. Kulkarni, R. J. Goldstein, *Energy separation in the wake of a cylinder: Effect of Reynolds number and acoustic resonance*, Int. J. Heat Mass Transfer **52** (2009), 3994–4000.
10. J. P. Gostelow, W. E. Carscallen, *Investigations of Eckert-Weise energy separation in the wakes of turbine blades and circular cylinder*, 17$^{\text{th}}$ Australasian Fluid Mechanics Conference 2010, Auckland, New Zealand.
11. J. M. Burazer, A. S. Ćoćić, M. R. Lečić, *Numerical research of the compressible flow in a vortex tube using OpenFOAM software*, Thermal Science **21**S3 (2017), S745–S758.
12. A. J. Favre, *The equations of compressible turbulent gases*, Annual summary report No I, Institut de Mechanique Statistique de la Turbulence, Marseille, France, 1969.
13. D. C. Wilcox, *Turbulence Modelling for CFD*, 2$^{\text{nd}}$ edition, DCW Industries, Inc. La Canada, California, 1994.
14. R. Issa, *Solution of the implicitly discretized fluid flow equations by operator splitting*, J. Comput. Phys. **62**, (1986), 40-65.
15. S. Patankar, D. Spalding, *A calculation procedure for heat, mass and momentum transfer in three-dimensional parabolic flows*, Int. J. Heat Mass Transfer **15** (1972), 1787–1806.
16. A. Kurganov, E. Tadmor, *New high-resolution central schemes for nonlinear conservation laws and convection-diffusion equations*, J. Comput. Phys. **160**(1) (2000), 241–82.
17. A. Kurganov, S. Noelle, G. Petrova, *Semidiscrete central-upwind schemes for hyperbolic conservation laws and Hamilton–Jacobi equation*, J. Comput. Phys. **160** (2000), 720–42.
18. C. Greenshields, H. Weller, L. Gasparin, J. Reece, *Implementation of semi-discrete, non-staggered central schemes in a colocated, polyhedral, finite volume framework, for high-speed viscous flows*, Int. J. Numer. Methods Fluids **63**(1) (2010), 1–21.
19. J. M. Burazer, *Turbulent compressible flow in a Ranque–Hilsch vortex tube*, Doctoral Dissertation, Faculty of Mechanical Engineering, University of Belgrade, 2017, UDC: 533.6.011.34:536.23:519.688(043.3), (in Serbian)

РАСЛОЈАВАЊЕ ПОЉА ТОТАЛНЕ ТЕМПЕРАТУРЕ ПРИ СТАЦИОНАРНОМ И НЕСТАЦИОНАРНОМ ОПСТРУЈАВАЊУ ЦИЛИНДРА

Резиме. Раслојавање поља тоталне температуре је последица спонтане прерасподеле тоталне енергије у струјном пољу. Као последица овог феномена, у струјном пољу постоје места са већом и мањом вредношћу тоталне температуре. Раслојавање поља тоталне температуре је карактеристично за многе струјне просторе. Овај рад се бави раслојвањем поља тоталне температуре у трагу опструјаваног цилиндра. Разматрају се два услова опструјавања цилиндра - нестационарно и стационарно. Два различита солвера из софтвера отвореног типа OpenFOAM се користе како би се успешно предвидело раслојавање поља тоталне температуре. Један од ових совлера је модификован специјално за прорачун нестационарног опструјавања цилиндра. Једначина енергије заснована на унутрашњој енергији, која је већ присутна у овом солверу је замењена једначином енергије која је записана преко тоталне енталпије. Други солвер је претходно тестиран у случају струјања у вртложној цеви, а може да предвиди раслојавање поља тоталне температуре и у стационарном опструјавању цилиндра. У оба случаја опструјавања цилиндра, коришћен је дводимензионални прорачунски домен. За прорачуне је коришћен стандардни $k-\varepsilon$ модел. Показано је да је помоћу OpenFOAM-а могуће предвидети феномен раслојавања поља тоталне температуре у оба случаја опструјавања цилиндра. У случају стационарног опструјавања цилиндра остварено је добро слагање између експерименталних и нумерички добијених резултата. Резултати претходних истраживања у случају нестационарног опструјавања цилиндра су такође потврђени.

Department of Fluid Mechanics
Faculty of Mechanical Engineering
University of Belgrade
Belgrade
Serbia
jburazer@mas.bg.ac.rs

(Received 30.11.2017.)
(Revised 17.05.2018.)
(Available online 24.05.2018.)